# A Comparison Between Observed Winds and Cloud Motions Derived from Satellite Infrared Measurements

WILLIAM E. SHENK AND EARL R. KREINS[1]

*Goddard Space Flight Center, Greenbelt, Md.*

(Manuscript received 4 December 1969, in revised form 21 April 1970)

ABSTRACT

Cloud motions were obtained from HRIR measurements contained within the overlapped region of two adjacent Nimbus II orbits. These 108-min averaged motions were compared with instantaneous wind vectors interpolated from constant pressure charts. Corrections for uncertainties in the attitude of the satellite were made by superimposing coastlines that were within the fields of view for both orbits. Cloud mass centroids were determined to estimate the position for each cloud. Cloud top altitudes were obtained from the Nimbus II HRIR data and the isotherms on the constant pressure charts. Generally, the direction and speed of the cloud motions were within 20° and 15 kt of the observed wind direction and speed.

## 1. Background

One of the fundamental measurements that must be made in defining the circulation of the atmosphere is the determination of winds at several levels with sufficient horizontal spacing. Present and planned efforts to accomplish this task are by tracking constant pressure balloons and by measuring the speed and direction of cloud movements as detected by visible and infrared sensing devices on board satellites placed in geosynchronous orbit. To date, only visible sensors have been placed in synchronous orbit on board the Applications Technology Satellites (ATS), and the reported research results indicate that judiciously selected small clouds can serve as atmospheric tracers. The most widely employed technique to obtain cloud motions from the ATS data is based on the ability to identify a cloud element on a series of successive photographs taken at intervals of ~20 min and then measure the cloud displacement from the first photograph to the last. Since the visible data provide no clear indication of cloud height, the clouds have been assigned to statistically determined preferred pressure levels (one each for low and high clouds) or to the pressure level where the conventionally observed wind most closely approximates the cloud motion. Generally, the results from these techniques have been the determination of wind direction to within 20° and speeds to within 10 kt. Infrared sensors placed in geosynchronous orbit should provide more definitive information on cloud top heights.

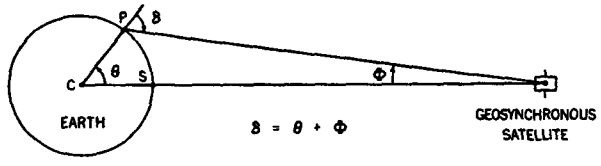


FIG. 1. Geometric relations between nadir angle $\phi$, local zenith angle $\delta$, and great circle arc $\theta$ for a satellite positioned in a geosynchronous orbit. Point P is an arbitrary point along the great circle, S is the subsatellite point, and C is at the center of the earth.

[1] Lieutenant Colonel, USAF, Air Weather Service, temporarily attached to the Goddard Space Flight Center. Present affiliation: Joint Meteorological Satellite Program Office, Headquarters USAF, Washington, D. C.

Most comparisons between cloud motions and wind observations have been performed within 50° of the great circle arc of the subsatellite point. Fig. 1 illustrates the geometric relations along a great circle passing through the subsatellite point between local zenith angle $\delta$, nadir angle $\Phi$, and great circle arc $\theta$. As the distance from the subsatellite point increases, a cloud is viewed more obliquely. As a result, greater difficulty is encountered in accurately identifying and locating a cloud element. Thus, it would be expected that cloud motions determined where $\delta$ is large would be less accurate and compare less favorably with the observed winds than where $\delta$ is small.

Fig. 2 shows the portion of the Northern Hemisphere that would be covered by four equally spaced equatorial geosynchronous satellites within three different limits of $\delta$. Coverage over North America was purposely given low priority since this is one region where conventional meteorological data are adequate. With a four geosynchronous satellite system complete coverage is assured to 30N within $\delta = 60°$. Let it be assumed that at $\delta = 60°$ the capability to determine winds from the geosynchronous satellite has dropped to the point

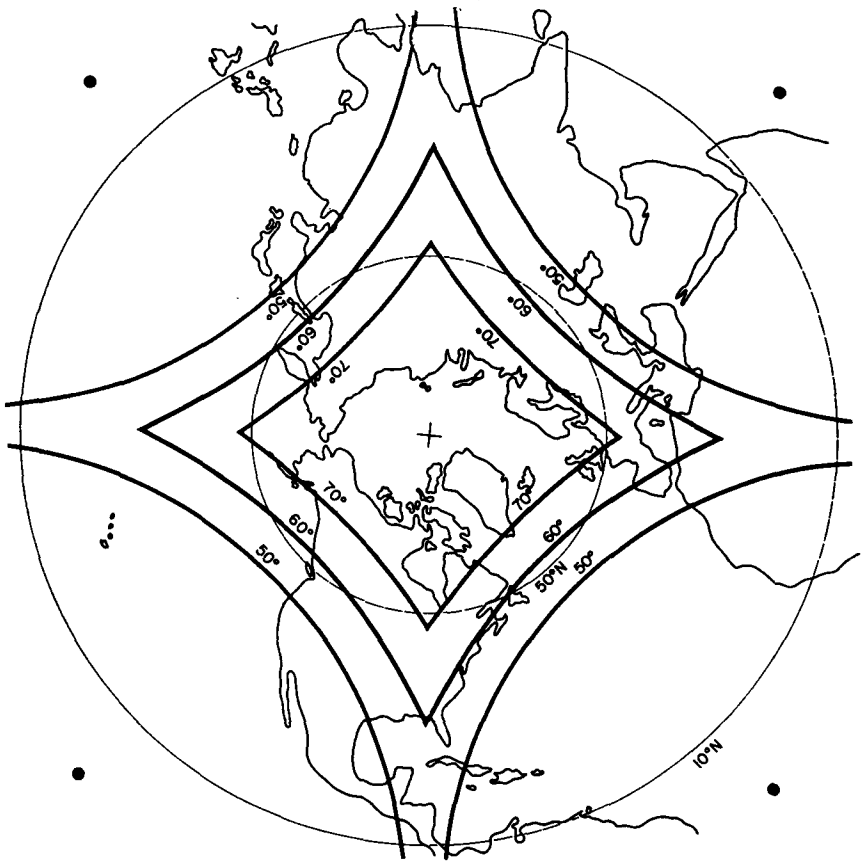


FIG. 2. Northern Hemispheric coverage with a system of four equatorial geosynchronous satellites. Curved lines are lines of equal $\delta$ relative to each subsatellite point and the black dots indicate each subsatellite point.

where alternate methods would receive strong consideration. Even with this four geosynchronous satellite system, cloud motion information would not provide accurate wind estimates over large areas of the North Atlantic and North Pacific Oceans. In the Southern Hemisphere, with its larger percentage of ocean surface to land surface, the oceanic data gaps would be more extensive.

The concept of wind measurement from satellites was mentioned before the launch of TIROS I (Widger and Touart, 1957). Greaves *et al.* (1965) tried to implement the concept by recognizing that there is considerable overlap in the data from adjacent orbits at high latitudes for satellites with highly inclined orbits. Using TIROS IX video data, the cloud displacements from one orbit to the next were computed after corrections were applied for parallax and for the attitude differences between orbits by matching recognizable landmarks in each orbit. These computed motion vectors were then compared with 500-mb geostrophic winds. The computed directions were generally within 30° of the observed direction except for three vectors where the average error was 140°. These three vectors were estimated from what were judged to be cirrus clouds well above the 500-mb surface. Generally, the computed speeds were substantially less than the 500-mb geostrophic winds with which they were compared. This effort suffered from the inability of the video data to locate the cloud at a specific level.

The above discussion illustrates several key points. First, the daytime visible data from the equatorial geosynchronous satellite may not be able to provide accurate wind measurements at large local zenith angles. Second, when the preferred levels technique is used, wind information is assigned to only two levels. Also, although the technique of obtaining winds from the video data in the overlapped region of the two adjacent orbits from a near polar orbiting satellite showed some promise, there was still an obvious need for better cloud top height estimates. Therefore, the ideal sensor to provide winds at high latitudes would be a polar orbiting satellite with sufficient resolution to see some cloud detail and give information on cloud top height. The High Resolution Infrared Radiometer (HRIR) on board the Nimbus I, II and III satellites comes closest to this ideal. For this study, the Nimbus II HRIR was chosen. Besides the search for a useful method for obtaining winds at high latitudes, this study also examines the general question of the feasibility of obtaining winds from radiometric measurements.

## 2. Nimbus II High Resolution Infrared Radiometer

The Nimbus II satellite was launched into a near-circular, retrograde, sun-synchronous polar orbit with an inclination of 100.3°, apogee and perigee heights of 1179 and 1095 km, respectively, and a nodal period of 108.17 min. A complete description of the spacecraft system is given in the Nimbus II Users' Guide (1966).

The HRIR sensed upwelling radiation in the 3.5–4.1 $\mu$ atmospheric "window" with a resolution of approximately 9 by 10 km at the subsatellite point. In this wavelength region, thermal emission and reflected solar radiation contribute about equally to the observed radiance during the daytime. However, at night when only thermal radiation is detected, reasonable meteorological interpretations of terrestrial radiation patterns can be made. The detected radiances, converted to equivalent blackbody temperatures, are used to determine surface temperatures, under clear sky conditions, and cloud top heights where the clouds are assumed to be opaque and completely fill the field of view of the radiometer.

The radiometer, which scanned perpendicular to the orbital track of the satellite, also sensed space radiance levels during portions of the scan. These space radiances were used as a threshold below which earth-sensed radiances could no longer be considered reliable. Since the average effective blackbody temperature associated with the space scans was between 220 and 230K, temperatures near or below these values must be interpreted cautiously.

The infrared data currently are available in two forms. One is a photographic image produced from the analog records. The other, a grid print map, is a computer display of the data rectified for various scales and map projections. More complete descriptions regarding these two types of data display can be found in the Nimbus II Users' Guide (1966) and in other publications such as Warnecke *et al.* (1968).

The measurements from the HRIR contained both periodic and random noise components. Spectral analysis revealed a strong 200-Hz noise component caused by interference from the spacecraft clock. This was largely removed by numerical filtering (McMillin, 1969).

Williamson (1969) has investigated the random noise of the HRIR measurements. He calculated the noise equivalent temperature difference, NE$\Delta T$, for the HRIR at several temperatures. For a radiometric measurement, NE$\Delta T$ is defined as the change in target temperature which would produce a change in measured response equal to the rms noise at the output of the instrument. Williamson found that for temperatures $<240$K the NE$\Delta T$ becomes large, even for data treated by McMillin's filter. In order to improve the temperature resolution at a given grid point on a grid print map, the number $N$ of digitized samples must be increased since the data error at any grid point is the error of any given sample divided by $N^{\frac{1}{2}}$. Some spatial resolution must be sacrificed if improved temperature resolution is desired.

## 3. Procedure

The first step was to select two adjacent orbits with HRIR coverage at high latitudes so that there was considerable overlap in the two data fields. A Mercator map projection with a scale of 1:2,000,000 was used to display the data. This scale gives a distance of 15 n mi between grid points at the equator and approximately 8 n mi at 60° latitude.

### *a. Data location*

Orbit-to-orbit random errors in data location, as much as 30 n mi, can occur from uncertainties in satellite attitude. This attitude error could result in sizable differences between apparent cloud motions and the corresponding observed winds. These errors were reduced by requiring distinguishable land features to be detectable in both orbits. These features can be matched and allowances made for the differences in attitude between orbits.

Another location error, caused by horizon location errors during the radiometer scan, is on the order of 3 n mi at the subsatellite point (Sabatini and Sissala, 1969). Since this error is much smaller than the attitude error and since there is no simple technique of correcting for it over large areas, no correction was applied.

Following the determination of the distance that one map had to be shifted to correct for attitude errors, individual cloud elements were selected that could be identified on both maps. Clouds that were in or very near surface frontal zones were avoided because of the expected sizeable influence of strong vertical motions near the front. Frontal zone clouds have the tendency to drift with the front and be poorly related to the winds moving through the front. Also, no cloud motion calculations were performed with the cloud top temperature $<240$K due to the nearness to the space threshold and the increase in random noise at cold temperatures. The centroid of each cloud mass was computed and the movement of the centroid from the earlier to later map was called the computed cloud motion.

Since the clouds were geographically placed by referencing the earth's surface and the clouds are above the surface, a parallax correction was applied to account for an apparent cloud motion from one orbit to the next. This correction was determined to be a 5 kt westward component for cloud tops $<500$ mb. As the correction would be less than this for cloud tops $>500$ mb, no correction was added in these cases.

### *b. Cloud top height determination*

There are several assumptions that are necessary in order to place a cloud top at a pressure level and to

geographically place the centroid. In the region where there is an apparent cloud, it is assumed that the cloud top surface completely fills the field of view of the radiometer and that the cloud is opaque. The failure of either assumption means that the apparent cloud top level is lower than the true level. To minimize the effect of these assumptions, the centroid was computed using the coldest region of the apparent cloud. A third assumption is that the cloud moves with the wind at the cloud top. Serebreny *et al.* (1969), comparing cloud motions computed from ATS pictures and observed winds, has indicated that this assumption is reasonable.

Another consideration in the vertical placement of the cloud tops is the temperature corrections that could be applied to the HRIR data due to the interference of atmospheric constituents. The principal interfering atmospheric constituents are carbon dioxide and water vapor. At the earth's surface over the range of nadir angles from 0° to 50°, corrections for these two constituents average about 3K (Warnecke *et al.*, 1969). Naturally, above the surface where the masses of carbon dioxide and water vapor are less, the corrections would be smaller. Since 3K corresponds to an average altitude error of about 0.3 km and most corrections would be smaller than 3K, no corrections were applied.

Instead of assigning the coldest individual value at a grid point within the area used to compute the centroid, a spatial average of several points was taken as representative of the effective cloud top temperature. The pressure level of the cloud top was determined to the nearest 25 mb by matching the effective cloud top temperature to the same temperature determined by interpolation from constant pressure charts at the standard pressure levels. Then the observed wind at the determined pressure level was interpolated from these conventional charts. Fig. 3 shows an example of two radiation data fields used to locate and identify a cloud element as well as the comparison between the computed cloud motion and the observed wind. The reader should note that the areas displayed in Fig. 3 are not geographically coincident. The figure depicts the relative motions of the cloud mass centroid from one orbit to the next.

*c. Data selection*

Synoptic situations were selected where most of the computed cloud motions were over water. Since the orbital period is 108 min, it becomes essential to minimize possible distortions in the cloud over this interval. Rough terrain influences changes in cloud shape, cloud height, and apparent motions due to preferred regions of cloud development and dissipation. Not only do these influences lead to erroneous cloud motions but they also increase the likelihood that a cloud will not be properly identified in the second orbit as the same cloud that was viewed in the first orbit.

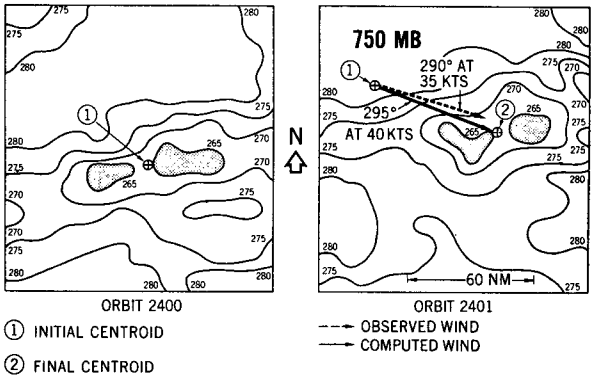


FIG. 3. An example of a cloud pair that was used to obtain cloud motion and the comparison with the observed wind. Isotherms are in °K.

Table 1 lists, for the cases studied, the orbital pairs, the midpoint time between the orbits, and the geographical features used to adjust for relative attitude errors.

Over and east of Asia, the Daily Weather Map series supplied by the Japan Meteorological Agency was the conventional meteorological data source used to extract the wind measurements and the temperature information necessary to fix the pressure level of the cloud top. This series contained charts at the mandatory levels from surface to 500 mb. Above 500 mb, National Meteorological Center (NMC) charts supplied the same information. Over North America, all interpolations were made from NMC mandatory level charts.

For the Asian synoptic cases, no observed wind interpolations were performed between the 1200 GMT constant pressure charts (closest time to the satellite passes) and the 0000 charts for the next day, except for one case. In this case, a rapidly moving shortwave trough was propagating through the area causing large wind fluctuations in a short time. Therefore, some adjustment was made to the 1200 GMT observed winds using the observed wind field displayed on the following set of 0000 charts. The midpoint times between each orbital pair were generally around 1500 (see Table 1).

Space and time interpolation was performed for the North American cases since the midpoint time for the adjacent orbits was about 0600 GMT.

TABLE 1. List of orbit pairs, midpoint time between orbits, and geographic features used to correct for relative attitude errors.

| Date | Midpoint time (GMT) | Data orbits | Geographic features |
|---|---|---|---|
| 15 September 1966 | 0530 | 1636,1637 | Great Lakes |
| 15 October 1966 | 1425 | 2040,2041 | Kamchatka Peninsula |
| 28 October 1966 | 0535 | 2208,2209 | Great Lakes |
| 1 November 1966 | 1545 | 2267,2268 | China Coast |
| 8 November 1966 | 1330 | 2360,2361 | China Coast |
| 10 November 1966 | 1410 | 2386,2387 | Kamchatka Peninsula |
| 11 November 1966 | 1530 | 2400,2401 | Kamchatka Peninsula |

TABLE 2. Pertinent data on cloud position, computed cloud top pressure level, computed and observed wind vectors, and cloud size and effective cloud top temperature on each grid print map for the case of 11 November 1966 at a midpoint time of 1530 GMT.

| Cloud no. | Midpoint of cloud position Latitude (N) | Midpoint of cloud position Longitude (E) | Computed cloud top pressure level (mb) | Computed cloud motion Direction (deg) | Computed cloud motion Speed (kt) | Observed wind Direction (deg) | Observed wind Speed (kt) |
|---|---|---|---|---|---|---|---|
| 1 | 48.5 | 146.5 | 850 | 300 | 25 | 305 | 25 |
| 2 | 45.5 | 144.0 | 700 | 310 | 25 | 295 | 35 |
| 3 | 42.0 | 138.0 | 750 | 290 | 40 | 290 | 30 |
| 4 | 41.5 | 136.0 | 750 | 295 | 40 | 290 | 35 |
| 5 | 39.5 | 135.5 | 450 | 275 | 65 | 280 | 70 |
| 6 | 37.5 | 131.5 | 425 | 285 | 60 | 270 | 60 |
| 7 | 33.0 | 132.5 | 600 | 255 | 40 | 275 | 30 |

| Cloud no. | First map (orbit 2400) Cloud size (n mi) | First map (orbit 2400) Effective $T_{BB}$ of cloud top (°K) | Second map (orbit 2401) Cloud size (n mi) | Second map (orbit 2401) Effective $T_{BB}$ of cloud top (°K) |
|---|---|---|---|---|
| 1 | 25×15 | 265 | 25×20 | 261 |
| 2 | 35×20 | 265 | 60×40 | 245 |
| 3 | 30×20 | 263 | 20×15 | 264 |
| 4 | 65×30 | 263 | 65×30 | 263 |
| 5 | 65 (cloud edge) | 240 | 80 (cloud edge) | 250 |
| 6 | 25×10 | 240 | 70×35 | 250 |
| 7 | 50×50 | 266 | 50×20 | 268 |

For a more detailed discussion of the procedure used by the authors, see Shenk and Kreins (1969).

## 4. Sample case

A complete discussion of one of the seven cases will be presented followed by a brief discussion of the highlights for the other six. The sample case to be discussed occurred 11 November 1966, with the midpoint time of 1530 GMT between the two adjacent orbits 2400 and 2401. Fig. 4 shows the amount of overlap in the HRIR data for the two orbits. Extensive portions of the China coastline and the Korean peninsula were clearly discernible in both orbits. A sharp 10K temperature difference between land and water marked the position of the China coast and a lesser difference was observed to indicate the Korean coastline. These temperature gradients were then superimposed and the amount of attitude error between orbits determined.

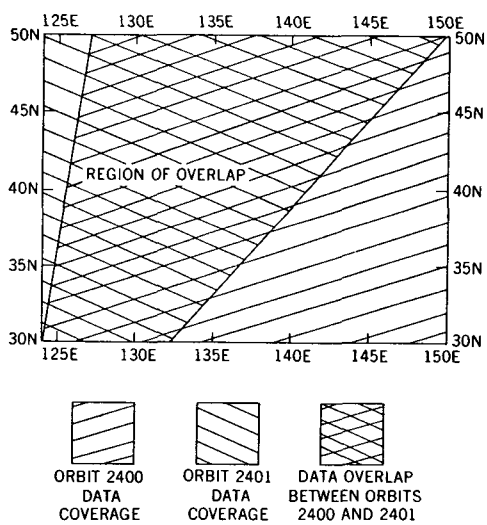


FIG. 4. The amount of overlap in data coverage in the HRIR data fields from two adjacent orbits (2400 and 2401) with a nadir angle limit of 50°.

Table 2 lists the appropriate information of each comparison made between the seven computed cloud motions and observed winds. Fig. 5 shows a schematic comparison of the computed vectors and the observed winds plus the determined cloud top levels. No adjustment in the observed winds was made between the conventional map time (1200 GMT) and the midpoint time for the two orbits. Five of the seven computed cloud motions were from the simple translation of a cloud element but the other two were attempts to use other techniques.

The first of these was a very prominent cloud edge. Fig. 6 shows two views of this cloud edge for the two orbits. As in Fig. 3, the areas shown in Figs. 6 and 7 are not geographically coincident. Instead of a centroid computation, the position of the edge was indicated at the midpoint of the edge and in the strongest thermal gradient. Selection of the appropriate temperature to vertically locate the cloud top was made subjective. This cloud edge appeared to be the leading edge of a middle and high cloud shield moving off the Asian coast. Since cirriform clouds form at least part of the shield, it seems plausible that the radiometer is viewing a cloud that is not completely opaque. Therefore, the observed HRIR gradient from east to west is probably due to an emissivity gradient rather than a substantial change in the height of the cloud or the amount of cloud filling the field of view of the radiometer. Thus, more weight was given in the cloud height determination to the effective temperatures well behind the cloud edge.

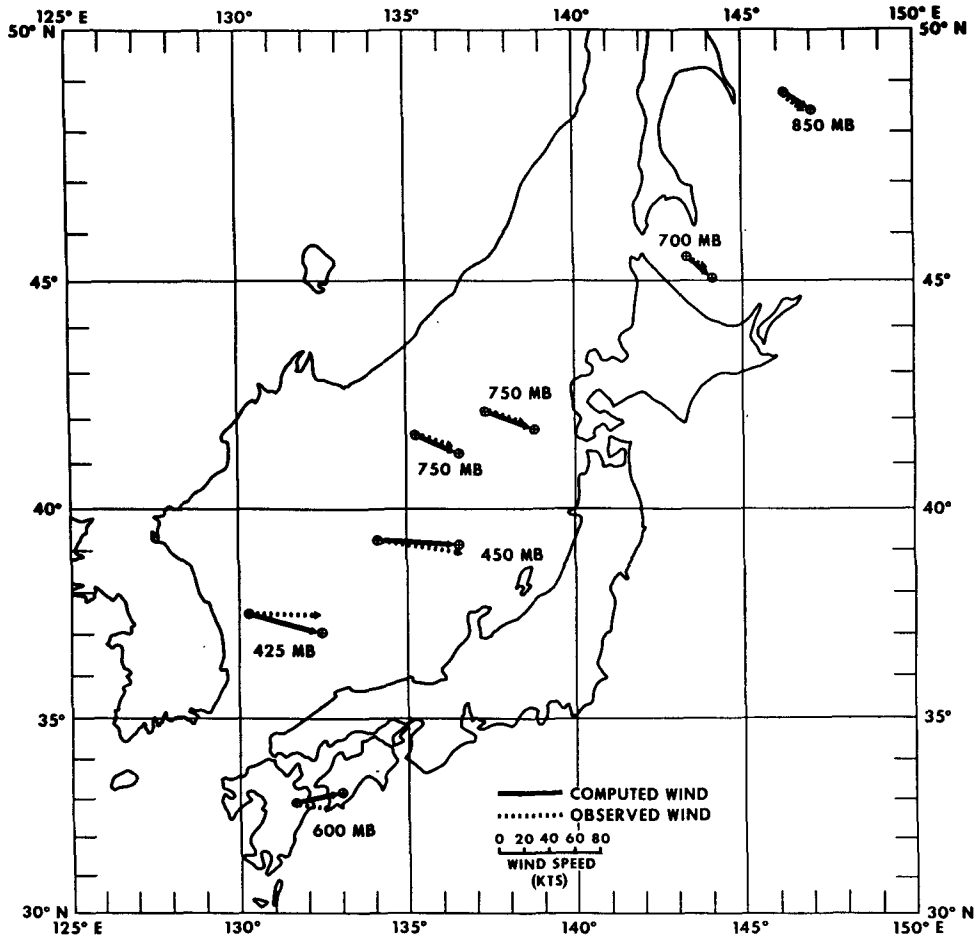


FIG. 5. Schematic presentation of the seven cloud motions and observed winds for the case of 11 November 1966. The cloud top heights are shown in mb.

Table 2 indicates that 245K was the average effective temperature selected. This estimate could easily be off by ±5K. The interpolated cloud top level was 450 mb and the computed cloud motion was 275° at 65 kt with a 5-kt westerly component being subtracted due to parallax. The interpolated observed wind at 450 mb was 280° at 70 kt.

Another technique was the use of a hole in the clouds. This hole, shown in Fig. 7 for the two orbits, was in the same general cloud mass that produced the prominent cloud edge to the northeast. The movement of the hole is controlled by the movement of the surrounding clouds. Therefore, the pressure "level" of the hole should be estimated from the surrounding cloud tops.

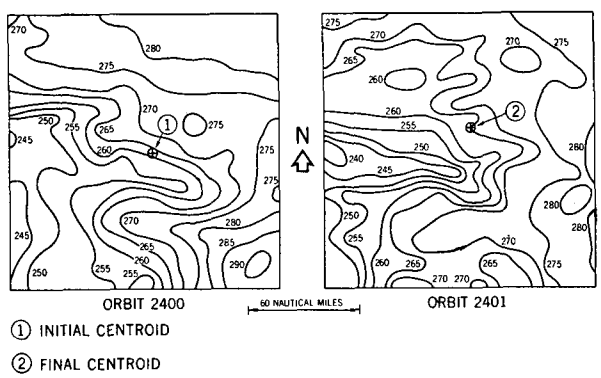


FIG. 6. Prominent cloud edge as shown in orbits 2400 and 2401. Isotherms are in °K.

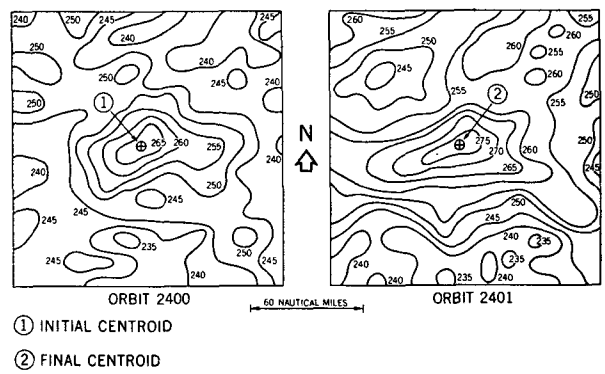


FIG. 7. Well-defined hole in an extensive cloud sheet (orbits 2400 and 2401). Isotherms are in °K.

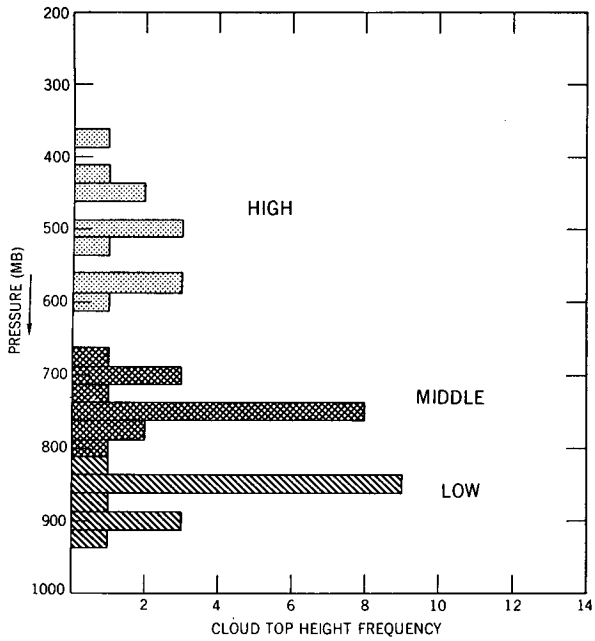


FIG. 8. Frequency distribution of cloud top heights. Class intervals are 25 mb.

A pressure level of 425 mb was assigned to the average effective temperature of 245K; the cloud direction and interpolated wind direction agreed to within 15°, while the cloud and observed wind speeds were the same (60 kt).

## 5. Highlights of the other cases

Of the remaining six cases, four were near the Asian Coast and the other two over North America. All of the computed cloud motions in the Asian cases were over water and all of the cloud vectors computed for the North American cases were over land. In addition to the simple translation of cloud elements, the centroid of an ensemble of small clouds was computed and the displacement of the ensemble measured. The comparison between the cloud motion and the concurrent wind was within 10° and 10 kt.

The greatest disparities between computed cloud motion direction and observed wind direction were noted in five computations which occurred over land between 850 mb and the surface. Four of the five cloud motions were computed for clouds over the Laurentian shield of eastern Canada and the fifth over the hilly terrain of northeastern Wisconsin. It is possible that there could be enough land influence on the clouds to cause the observed directional differences of 30°–40°. These five vectors will be specially considered in the statistical analysis in the next section.

## 6. Statistical analysis

Fig. 8 shows the frequency distribution of the cloud top heights. A trimodal distribution is suggested, reflecting some tendency for clouds to be either low, middle or high.

Fig. 9 is a cumulative frequency diagram for the entire data sample which shows the numerical change in the effective blackbody temperature from the first to the second view of each cloud. There was only a 3K change in the cloud top temperature in 108 min for over 60% of the clouds used as tracers. The majority of this amount of temperature fluctuation could be caused simply by viewing the cloud at different nadir angles from one orbit to the next. Over 85% of the clouds had an effective blackbody temperature change $\leq$6K. Of the five clouds with orbit-to-orbit effective blackbody temperature changes >7K, two of these were a cloud edge pair and the hole in the clouds. These results suggest that little convective activity was connected with the tracer clouds. This is not surprising since the clouds were sensed at high latitudes where minimal convective activity would be expected. The small temperature changes also indicate that nonconvective cloud top temperatures tend to be conservative with time.

Figs. 10 and 11, respectively, show plots of computed cloud direction vs observed wind direction and computed cloud speed vs observed wind speed. The 45° angle line in both figures represents a perfect correlation. The cloud motions where substantial topographical influence is suspected are labelled with an X. Since a high percentage of winds have a westerly component, there is a bunching of the data points between 220° and 320° in the direction scatter diagram. The scatter appears to be about equally divided on either side of the perfect correlation line. Thus, no consistent directional bias in the computed cloud motions is present.

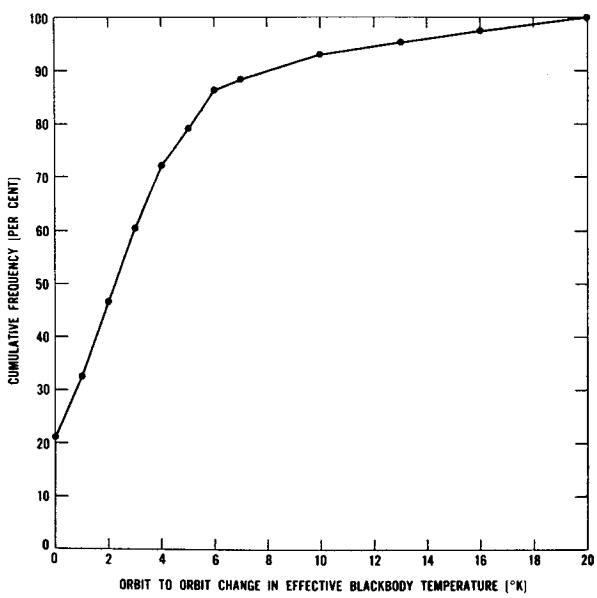


FIG. 9. Cumulative frequency diagram of the orbit-to-orbit change in the effective blackbody temperatures of the cloud tops.

In the speed scatter diagram, there is a slight tendency for the computed speeds to be higher than the observed speeds (by an average of 3.1 kt). This effect may be due to cloud propagation. More likely, it reflects the inability of the radiometer to verify that the field of view is completely cloud filled and that the cloud top is not completely opaque. These latter effects mean that some of the contributed radiance to the total sensed radiance is emitted from within or below the cloud. The results of these effects are that the true cloud tops are probably higher than those indicated by the radiometer. The opacity effect is probably greatest where the clouds are close to the cirrus level. Kuhn and Weickmann (1969) have reported that emissivities associated with cirrus are substantially less than 1.0. Thus, since the wind speeds normally increase with height below the tropopause, the observed wind speeds would have more closely approximated the cloud speeds at some higher level.

Table 3 is a tabulation of the absolute magnitude of the direction and speed differences between the observed wind and the computed cloud motions for three classes of apparent cloud size as measured by the length of the major axis of the cloud. The table shows that there is a gradual increase in the average direction difference as the major axis of the cloud becomes greater, but a decrease in the average speed difference with increasing major axis length. Thus, the average vector difference was not very dependent on the size of the cloud used as a tracer.

Court (1958) and Durst (1954) have developed statistical relations to compute vector correlation coefficients. Court's total vector correlation coefficient $R_{wz}$ is more complete than Durst's coefficient $r_{wz}$. Court's relation involves multiple correlation of the variables while Durst's is like the simple correlation of two variables.

Two computations of $R_{wz}$ and $r_{wz}$ were performed. One set of computations was with the full data sample

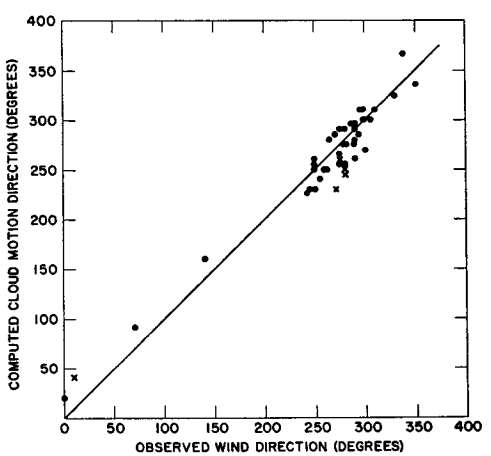


FIG. 10. Scatter diagram of computed cloud motion (direction) vs observed wind direction.

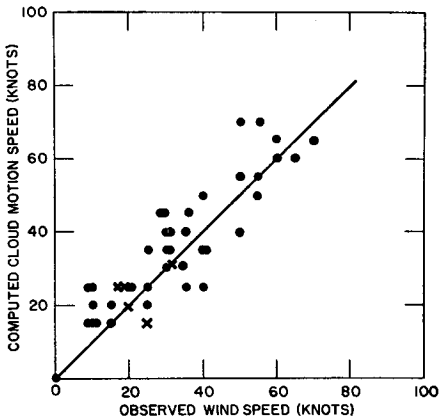


FIG. 11. Scatter diagram of computed cloud motion (speed) vs observed wind speed.

(43 pairs) and the other excluded the five pairs where topography possibly influenced the clouds. The results for each sample were identical, $R_{wz}=0.85$ and $r_{wz}=0.84$. The fact that $R_{wz}$ and $r_{wz}$ were the same for the two samples shows that even though there was a relatively large error in direction between the low-level cloud motions and observed winds over hilly terrain, the small speed errors compensated.

There is no rigorous way to estimate the confidence limits for Court's $R_{wz}$. However, Court[2] suggested that a Fisher $z$ transformation should be useful in testing the significance of linear correlation coefficients. In application of this test, comparison is then made with the normalized standard deviation $\sigma_z$ equal to $1/(2N-10)$,

TABLE 3. Frequency of occurrence of the number of cases where the absolute magnitude of the direction and speed differences between the observed wind and the computed cloud motions fell in given ranges for various apparent cloud sizes.

| Cloud size (major axis) (n mi) | Direction difference (deg) 0 | 5 | 10 | 15 | 20 | 25 | 30 | 35 | 40 | Average direction difference (deg) |
|---|---|---|---|---|---|---|---|---|---|---|
| 20–40 | 4 | 3 | 3 | 2 | | 1 | | 1 | 1 | 11.7 |
| 45–70 | 1 | 3 | 4 | 8 | 4 | 1 | 2 | | | 14.8 |
| >70 | | 1 | 1 | | 1 | | 2 | | | 19.0 |
| Total number | 5 | 7 | 8 | 10 | 5 | 2 | 4 | 1 | 1 | 14.2 |

| Cloud size (major axis) (n mi) | Speed difference (kt) 0 | 5 | 10 | 15 | 20 | Average speed difference (kt) |
|---|---|---|---|---|---|---|
| 20–40 | 2 | 5 | 5 | 2 | 1 | 8.3 |
| 45–70 | 5 | 11 | 4 | 3 | | 6.1 |
| >70 | 1 | 3 | | 1 | | 6.0 |
| Total number | 8 | 19 | 9 | 6 | 1 | 6.9 |

[2] Personal communication, 1969.

where $N$ represents the number of independent data pairs.

In the use of the $z$ transformation, the null hypothesis is that the correlation between the two populations is zero. The probability that the observed correlation between the samples could be due to accidental sampling is determined. In this study, it is assumed that the distribution of sample correlation coefficients that could be computed by further studies in not normal. This is a conservative view. The transformation $z$ is given by $z=1/2[\ln(1+r)-\ln(1-r)]$, where in this case, $r=R_{wz}$. As often is the case in meteorology, estimating the number of degrees of freedom is not straightforward. One sample contained 43 pairs and the other 38. However, the number of degrees of freedom is undoubtedly smaller due to spatial dependence between sample pairs within a given synoptic situation and some intercorrelation between synoptic situations. The number of degrees of freedom as suggested by Court is $2N-10$. A conservative hypothesis would be to assume that the seven synoptic situations are independent but that there is perfect correlation between pairs within each situation. A more reasonable degree of freedom estimate probably lies in between this extreme and the extreme of complete pair independence. It was assumed that within any synoptic case, exactly two pairs were independent of one another (rather than the average number of six pairs). Thus, the number of degrees of freedom, $2N-10$, is 18. The Student's $t$ test relation is expressed as $t=z/\sigma_z$ which equals 5.48. For 18 degrees of freedom this value of $t$ indicates that the probability of the correlation coefficient originating from an uncorrelated population would be less than 0.1%.

## 7. Conclusions

The primary conclusion of this investigation is that by using Nimbus II HRIR data from two adjacent orbits, it is possible to obtain representative cloud motions that correlate reasonably well with the observed winds. A substantial contribution to this positive result was undoubtedly the radiometer capability to more clearly determine cloud top height than is possible with visible data. This capability, at least in part, compensated for the poorer spatial and time resolution than is currently available in computing cloud motions from the ATS satellite visible data. Since the overlap between adjacent orbits is most significant at high latitudes, this technique might be most useful in the determination of winds over high latitude oceanic regions. It follows that it should be possible to derive wind data from other radiometric measurements where the resolution and noise characteristics are the same or better than the Nimbus II HRIR. This is important since there are active programs to place radiometers in geosynchronous orbit with the wind measuring capability as the primary scientific objective. Results as good as or better than the above should be anticipated from geosynchronous altitude in view of the shorter interval between successive views of a cloud element. The restrictions that the effective blackbody temperature be limited to 240K or greater and that distinguishable land features are detectable in both orbits were imposed by the characteristics of the Nimbus HRIR and the uncertainties in satellite attitude, respectively. It is anticipated that these restrictions to the technique discussed in this paper can be removed with the advent of infrared sensors with improved temperature resolution and improved satellite attitude determination, both of which are being considered for future meteorological satellites.

*Acknowledgments.* We are indebted to Dr. Frank L. Martin for his suggestion of computing the vector correlation coefficients and to Mr. William R. Bandeen for his careful scrutiny of the manuscript. Also, we appreciated the stimulation of constant discourse with numerous other members of the Planetary Radiations Branch of the Laboratory for Atmospheric and Biological Sciences.

REFERENCES

Court, A., 1958: Wind correlation and regression. Sci. Rept. No. 3, Cooperative Research Foundation, San Francisco, Calif., 16 pp.

Durst, C. S., 1954: Variation of wind with time and distance. *Geophys. Mem.*, No. 93, Meteorological Office, Air Ministry, London, England.

Greaves, J. R., J. C. Barnes, W. P. Smith and W. K. Widger, Jr., 1965: Cloud feature persistence in satellite pictures and its applicability to wind determination. ARACON Geophysics Co., Concord, Mass., Final Rept., Cwb-10988, 42 p.

Kuhn, P. M., and H. K. Weickmann, 1969: High altitude radiometric measurements of cirrus. *J. Appl. Meteor.*, **8**, 147–154.

McMillin, L. M., 1969: A procedure to eliminate periodic noise found in Nimbus II High Resolution Infrared Radiometer measurements. Allied Research Associates, Inc., Concord, Mass., Tech. Rept. No. 9, Contract NAS5-10343, 16 p.

Nimbus Project, 1966: *Nimbus II Users' Guide.* Goddard Space Flight Center, Greenbelt, Md., 229 pp.

Sabatini, R. R., and J. E. Sissala, 1969: Nimbus earth resources observations. Allied Research Associated, Inc., Concord, Mass., Tech. Rept. No. 7, Contract NAS5-10343, 67 p.

Serebreny, S. M., R. G. Hadfield, R. M. Trudeau and E. J. Wiegman, 1969: Comparison of cloud motion vectors and rawinsonde data. Final Rept., ESSA Contract E-193-68, Stanford Research Institute, Menlo Park, Calif., 30 p.

Shenk, W. E., and E. R. Kreins, 1969: A comparison between observed winds and cloud motions derived from Nimbus II HRIR measurements. Goddard Space Flight Center, Greenbelt, Md., X-622-69-285, 43 p.

Warnecke, G., L. J. Allison, E. R. Kreins and L. M. McMillin, 1968: A satellite view of typhoon Marie 1966 development. Goddard Space Flight Center, Greenbelt, Md., NASA TN D-4757, 94 p.

——, L. M. McMillin and L. J. Allison, 1969: Ocean current and sea surface temperature observations from meteorological satellites. Goddard Space Flight Center, Greenbelt, Md., NASA TN-D-5142, 47 p.

Widger, W. K., Jr., and C. N. Touart, 1957: Utilization of satellite observations in weather analysis and forecasting. *Bull. Amer. Meteor. Soc.*, **38**, 521–533.

Williamson, E. J., 1969: The accuracy of the High Resolution Infrared Radiometer on Nimbus II. Goddard Space Flight Center, Greenbelt, Md., NASA TN-D-5551, 14 p.